Geomechanical Properties of Coal Macerals; Applications Towards Modelling Swelling of Coal Seams During Carbon Sequestration

Thomas Fender[a], Mohamed Rouainia[b], Cees Van Der Land[a], David Martin Jones[b], Maria Mastalerz[c], Jan A. I. Hennissen[d], Samuel Graham[b], Thomas Wagner[e]

[a]School of Natural and Environmental Sciences, Newcastle University, Newcastle-Upon-Tyne, NE1 7RU, United Kingdom
[b]School of Engineering, Newcastle university, Newcastle-Upon-Tyne, NE1 7RU, United Kingdom
[c]Indiana Geological and Water Survey, Bloomington, Indiana, IN 47405, United States
[d]British Geological Survey, Keyworth, Nottingham,NG12 5GG, United Kingdom
[e]Lyell Centre, Heriot Watt University, Edinburgh, EH14 4AS, United Kingdom

Abstract

Understanding the mechanical response of coal to CO_2 injection is a key to determine the suitability of a seam for carbon capture and underground storage (CCUS). The bulk elastic properties of a coal, which determine its mechanical response, are controlled by the elastic properties of its individual components; macerals and minerals. The elastic properties of minerals are well understood, and attempts have been made to acquire maceral elastic properties (Young's modulus) by means of Nanoindentation. However,due to the resolution of a nanoindent; the response is likely to be a combination of macerals. Here Atomic Force Microscopy is used for the first time to give a unique understanding of the local Young's modulus of individual coal macerals, with a precision of 10nm in both immature and mature coals. The results at this length scale indicate that the mean and modal Young's modulus values in all macerals is less than 10GPa. Thermally immature liptinite macerals have a lower modal modulus than the equivalent inertinites. The modulus response is also non-normally distributed and most likely conform to a gamma distribution with shape parameter between 1.5-2.5. The modal Young's modulus of all macerals increases with maturity, but not at the same rate, whereby the liptinite macerals become stiffer than the inertinites by the gas window. The difference between liptinite and inertinite modulus values is greater within immature coals than mature coals. Modelling of volumetric strain under CO_2 injection indicates an inversely proportionate relationship to Young's modulus, which suggest that differential swelling is more likely to occur in immature coals. As such it is preferential to target mature coals for CCUS, as the reaction of macerals at higher maturities is more predictable across an entire coal seam.

Keywords: Atomic Force Microscopy, Maceral, Young's modulus, Carbon Sequestration, Coal Swelling, Inertinite, Liptinite

2010 MSC: 00-01, 99-00

Email address: t.fender1@newcastle.ac.uk (Thomas Fender)

1. Introduction

As the world moves toward a net-neutral carbon environment, further emphasis has been put on undertaking carbon capture and underground storage (CCUS). Advances have been made in re-purposing former conventional hydrocarbon reservoirs in; the Norwegian Continental Shelf with the Sleipner storage facility, amongst others (Bickle, 2009; Cavanagh and Ringrose, 2014), the Weyburn oilfield, Canada (Zaluski et al., 2016, and references therein) and Al Salah, Algeria (Ringrose et al., 2009; Mathieson et al., 2010) Meanwhile, recoveries from many current conventional and unconventional hydrocarbon reservoirs are being enhanced with CO_2 injection across the world. This technique has proven successful in the Permian Basin of North America, helping to both extract residual oil and offset the carbon footprint of a major conventional oil play (West, 2014).

Conventional oil and gas reservoirs make appropriate locations for storage of CO_2 underground due to preexisting knowledge of their geological conditions as well as reservoir production data obtained during the field's lifetime. Deep coal deposits represent another potenital target for storage of supercritical liquid and gaseous CO_2. Currently CCUS is actively occurring within deep coal seams within the San Juan Basin, USA (Weber et al., 2012); Alberta, Canada (Gentzis, 2000); and the Qinshui Basin (Wang et al., 2016) and Yaojie Coalfield (Li et al., 2013), China.

Coal has a natural CO_2 storage capacity, with an intrinsic affinity for adsorbing carbon dioxide onto its porous surfaces, and porosity can be 50 cm^3/g (Laxminarayana and Crosdale, 1999). Sorption of CO_2 into coal has been widely studied (Liu et al., 2010; Masoudian, 2016; Ranjith and Perera, 2012) with coal seams acting as naturally fractured reservoirs, combining both fracture porosity with the natural micro (<10 nm) and meso (<100 nm) porosity that exists within the coal body itself (Espinoza et al., 2015).

Whilst the effects of injecting supercritical CO_2 into conventional clastic reservoirs are relatively well understood, the intrinsic problems with swelling of coals complicates matters greatly. Coals are known to swell under CO_2 injection (Levine, 1996; Robertson, 2005), which initially leads to the opening of fractures and increased permeability (Pan and Connell, 2007). Further injection leads to a two fold impact on permeability. Firstly the increase in CO_2 volume causes further swelling opening up fractures increasing permeability, which is secondly followed by an increase in pore fluid pressure decreasing permeability (Pan and Connell, 2007; Pan et al., 2010).

When attempting to model the impact on coals of injecting of CO_2, several mechanical properties are integral to our understanding of how this poro-elastic framework works. The most frequent mechanical properties required are Young's modulus, Poisson's ratio and bulk modulus (Pan and Connell, 2007; Palmer et al., 1996; Shi and Durucan, 2004); all of which can be calculated through mechanical property testing (e.g. triaxial).

Triaxial measurements of coal Young's modulus and Poisson's ratio are widely variable and are influenced greatly by pore-pressure and effective stress (Gentzis et al., 2007; Pan et al., 2010; Espinoza et al., 2015), whilst Alexeev et al. (2004) suggest that triaxial tests undertaken on steeply dipping coals should be done with a non-uniform stress state, to compensate for the inclined bedding direction. The water content of coal

has been observed to affect triaxial and nanoindentation derived Young's modulus greatly (Alexeev et al., 2004; Zhang et al., 2018b), with increasing water content drastically decreasing coal integrity. Any techniques that help elucidate the complex relationships that exist between coal mechanical properties, strain and permeability must be investigated further.

Triaxial testing whilst keeping either a constant pore water pressure or constant mean effective stress has been used to derive the stress/strain and pore water pressure/strength relationships, allowing for modelling of these relationships under different CO_2 injection pressures (Pan et al., 2010; Espinoza et al., 2015). Triaxial results and modelling indicate there is a non-linear relationship between effective stress and strain/ shear strength. Possion's ratios have been reported in the region of $0.22 - 0.48$ from triaxial testing and sonic velocities (Zheng et al., 1991; Gentzis et al., 2007; Ranathunga et al., 2016). Reported Young's modulus values of coal from triaxial experiments vary drastically, with values appearing to be within the region of as 40-70MPa reported (Viete and Ranjith, 2006; Ranathunga et al., 2016) for coals with significant water content, however Gentzis et al. (2007) report moduli as high as 5.07GPa.

Vickers hardness testing is higher resolution than triaxial testing (mm^3 rather than cm^3) (Figure 1), ignoring larger cleats and fractures, while the Indentation modulus of individual macerals is an order of magnitude higher than the values obtained by most triaxial testing; Stach et al. (1982) reporting a variation between $240 - 382$MPa on vitrinite. Other Vickers hardness testing on coals report an increase in hardness with coal rank and as such carbon content. Microhardness observations from the Vickers test account for both plastic and elastic behaviour, with coals having a reported microhardness of 20–100 kg/mm^2 (Hower et al., 2008, and references within), with the hardness associated with vitrinite reported as 24.5-36.6kp/mm^2 (Stach et al., 1982).

Higher resolution nanoindentation studies (~ 10s of $microns^3$) (Figure1) have been undertaken on coals, and report a variety of Young's moduli and hardness values, between 3.02GPa and 9.04GPa, with many authors reported modulus values of 4–7GPa (Yu et al., 2018; Borodich et al., 2015; Epshtein et al., 2015; 2016; Zhang et al., 2018b). This variation in moduli accounts for a variation in vitrinite reflectance of 0.4%–1.52%R_o. The resolution of nanoindentation is on the order of $1 - 15\mu m^3$ and thus removes the effects of cleats and larger fractures, allowing increased accuracy in measurements of undamaged coal matrix effective modulus.

Obtaining local elastic moduli of coal and coal macerals proved to be relatively difficult due to the size of some macerals and regular distribution of nanoscale porosity in both nano and meso-sized pores. However, technical advances in Atomic Force Microscopy (AFM) in the last few years, now allow increased insight into these properties and enable thousands of high resolution measurements in a timely manner (Figure 1). One of the first studies using AFM to understand coal at higher resolutions was undertaken by Li et al. (2020) using a PeakForce™QNM™AFM. These results indicate a Young's modulus distribution with peaks at 8GPa, 11GPa and 14GPa, with a bimodal distribution found in one sample, but normally distributed in

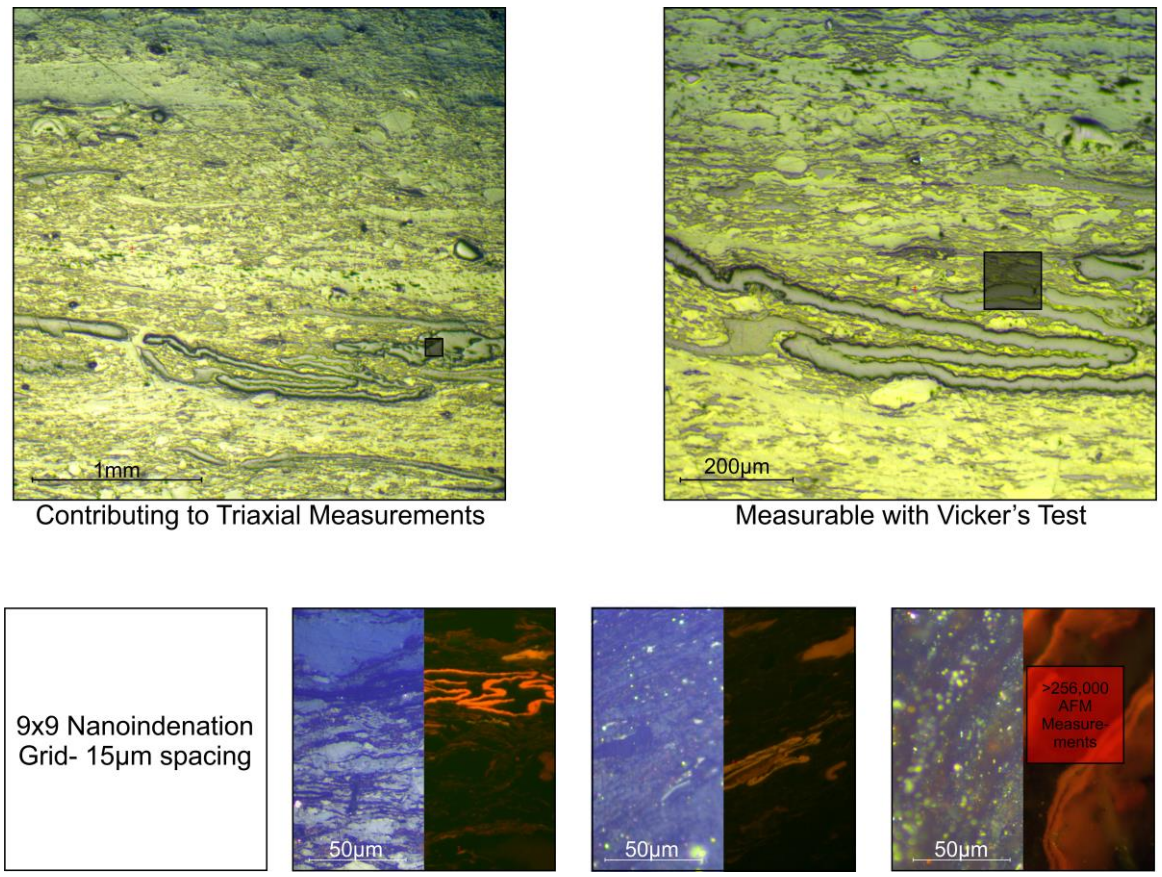

Figure 1: An indication of the scale in which coals can be analysed by Triaxial, Vickers microhardness tests, Nanoindentation and AFM. The black box is the area in which a 9x9 nanoindentation grid would be situated. The red box is the area of one AFM scan within this study, containing over 250,000 measurements.

others. The occurence of a bimodal distribution was assumed to be due to mineral matter, with a softer pure organic peak and stiffer organic/mineral peak (Li et al., 2020). This represents the first acquisition of true non-effective, local Young's moduli of coal.

Shale mechanical properties, although not as readily important on the injection of CO_2 in conventional reservoirs, become important properties of the shales that cap most appropriate conventional CCUS reservoirs. The mechanical properties of coals and shales are therefore a first order control on the feasibility of CO_2 injection and long term storage within most conventional and unconventional targets.

AFM has been used for the last 5 years to obtain Young's modulus results at the resolution required for coal maceral analysis on shale organic matter indicating a variation from <1GPa to ~ 32GPa as well as identifying a bimodal distribution in organic matter, and a stiffening with maturity (Eliyahu et al., 2015; Emmanuel et al., 2016; Goodarzi et al., 2017; Li et al., 2018; Khatibi et al., 2018). Here we undertake a similar approach to identify trends within similar organic matter in coals.

1.1. Maceral Analysis

Coals and organic rich shales are compositionally made of mineral and organic phases. In coals the mineral phase is generally less than 50% of the sample by weight. The organic phase in shales tends to be between 1 and 10% of the whole rock by weight (Stephen and Passey, 1993; Jarvie et al., 2004).

Organic matter in shales is commonly categorised on provenance (e.g. terrestrial/ marine/ lacustrine) or derived from Rock Eval Pyrolysis (Type I, Type II, Type III, Type IV), whereas in coals this classification differs in that it is based more heavily on the organic precursor (e.g. cutin, lignin). Whilst it is convenient to describe organic matter in shales in terms of provenance, shales can also be described in terms of precursor. It may offer insight into the geolocial and geomechanical processes to define the organic matter in shales by the same classifications as those for coal, more specifically into the three main maceral groups from Stach et al. (1982).

Liptinite is derived from plant and algal remains rich, in hydrogen. Vitrinite is sourced from hydrogen lean structural components of plant remains, whilst inertinite is oxidised or biochemically altered liptinite and vitrinite (O'Keefe et al., 2013). Each of these maceral groups can be further subdivided, however, only liptinite can be subdivided based truely on precursor material (Stach et al., 1982), whereas inertinite and vitrinite are mainly divided based on the oxidiser of the originial structure and the extent of oxidation. In low rank coals liptinite macerals are defined by low relief and high fluorescence (Stach et al., 1982; Teichmüller, 1989). Liptinite has four main subgroups:

- cutinite, derived from leaf cuticles which contain abundant fatty acids and waxes used by plants to protect from oxidation;
- sporinite, the remnants of spores and pollen, generally comprising just the exine;
- alginite; remnants of algal material;

- resinite, derived from resins, balsams, latexes, fats and waxes (Teichmüller, 1989);
- Lastly liptodetrinite is any liptinite maceral that cannot be assigned to any of the groups above, mainly because of its small size (Stach et al., 1982).

Shales do have some macerals that are present in coal, but are usually dominated by amorphous organic matter (AOM), that can occur as layers or granular material admixed into the matrix. Other macerals are also present within some shales though, alginite is another a key component in some of the most prolific black shales (e.g. Green River Shale (Ingram et al., 1983)).

Coal macerals are generally less than 100 μm in size and as such very little effort has been made to study how these individual components of a coal influence the overall mechanical properties (Borodich et al., 2015). It is important to establish whether these structured groups are load supporting. Here we present some of the first work to classify coal and shale macerals mechanical properties. This provides insight into the interactions between macerals upon increased stress from CO_2 injection and the associated swelling.

2. Methods and Samples

2.1. Samples and Preparation

Three samples of coal and one of shale were selected for this study due to being rich in a particular maceral. The paper Coal rich in cutinite, cannel Coal rich in both alginite and for the purposes of this study sporinite, New Albany shale rich in alginite and a oal from the Northumberland coal field, rich in both vitrinite and inertinite.

The paper coal and cannel coal come from the eastern part of the Illinois Basin, and are Pennsylvanian in age. Both samples are associated with the Upper Block Coal Member in Indiana and were likely deposited in deltaic-fluvial dominated environment (DiMichele et al., 1984).

The Northumberland coal was deposited in the North East of England in the Northumberland Basin during the Pennsylvanian. This basin formed from subsidence associated with early Carboniferous rifting and the associated thermal sag (Turner and Richardson, 2004; Murchison, 2004; Leeder, 1988). The coals were deposited as part of an alluvial succession with a thickness of 750m (Turner and Richardson, 2004). The environment of deposition was a vast alluvial plane fed by sediment from the North and North East, carried by low gradient rivers to the south and southwest. The prodelta top sediments mainly comprised peat and other Carboniferous vegetation, which once lithified became the well-known Northumberland Coal seams used to power Britain for much of the 20th century (Turner and Richardson, 2004). Of the coal deposited in the Pennsylvanian, only the Pennine Lower and Middle Coal Measures are present in Northumberland.

A sample of coal from the Top Plessey seam, which is part of the Pennine Middle Coal Meaures indicated in (Bullock et al., 2018) has been collected in-situ from the exposed seam at the Shotton Surface Mine, Cramlington. Reported vitrinite reflectance measurements for this seam are between 1.3-1.6%R_o (Bullock

Coal	Mean Vitrinite Reflectance (%)
Cannel Coal	0.38
Paper Coal	0.39
Northumberland Coal	1.56

Table 1: Mean mesured vitrinite reflectance values for the coals studied from 100 point counts.

et al., 2018), indicating that this coal is of a rank between medium-low volatile bituminous coal (Stach et al., 1982).

The New Albany Shale sample is upper Devonian and comes from a core (543m depth) drilled in Daviess County, Indiana. The New Albany Shale is Type II kerogen sequence ranging in mature from immature to post mature (Strapoc et al., 2010). The sample studied has R_o of ~ 0.65%, thus representing early stage thermal maturity (Mastalerz et al., 2016).

Coal samples from the paper and cannel coal were then crushed and mounted in epoxy resin before being polished to a flat surface using 0.5μm alumina powder (Taylor et al., 1998). The Northumberland coal was cut perpendicular to bedding and mounted in epoxy resin and polished using the same technique. The sample of New Albany Shale was prepared as a kerogen isolate slide; initially treated with hydrochloric acid and hydrofluoric acid to remove carbonate and silicates (Rexer et al., 2014), then filtered through a 10μm sieve and strewn-mounted on microslides coated in resin.

2.2. Maceral analysis

Maceral identification was undertaken initially without immersion oil due to the possibility of remnant oil on the surface intefering with the AFM QI™ analysis. A Leica DM2700 P™ polarising microscope at 400× and 630× magnification was used to identify the macerals.

Slides were also studied in blue light excitation following the standard recommendations for epifluorescence on coal polished blocks (Taylor et al., 1998). Once scanned with the AFM, final images of each maceral were taken at 500× magnification under immersion oil for analysis of AFM scan location.

Vitrinite reflectance was measured on the samples of cannel, paper and Northumberland coal using the Leica DM2700 P at 500× magnification. This was undertaken using reflectance standards at 0.42, 0.69 and 0.91%R_o on 100 individual particles of vitrinite for each coal (Taylor et al., 1998). The mean values are reported in Table 1 removing any perceived outliers. Vitrinite reflectance measurements were conducted in accordance with the method presented in Standard et al. (2014).

2.3. Atomic Force Microscopy Quantitative Imaging

Atomic Force Microscopy Quantitative Image™ (AFM QI™) was undertaken on a JPK Nano Wizard 3 in QI™ mode (Instruments, 2011). RTESPA-525 silicon nitride tips were selected for this experimental set-up, with a reported working range of <1GPa- ~ 25GPa (Pittenger et al., 2014), however, accurate

measurements of up to 30GPa have been reported using the previous generation of these tips by Emmanuel et al. (2016).

The mechanism of AFM QI™ involves the oscillation of a tip onto the sample surface by a cantilever at a frequency below its resonance frequency. The force applied to the sample is set (in this case to 500nN), and the displacement is in the order of 1-3nm. This is measured by a current generated from the deflection of a laser beamed off the head of the tip onto a photo-diode. The radii of the tips used in this study are reported to range between 8-12nm, although 10nm was used as the average tip radius for processing of Young's modulus data.

One cycle of AFM QI™ scanning is described in Figure 2, in which the tip is brought towards the sample from a point 150nm away, until a point (b) where adhesive Van Der Waals forces cause the tip to flex onto the sample surface. At a point of maximum adhesion (c) a force is emparted onto the sample surface by the tip. The deflection measured at the point (d) of maximum force (500nN). The extend curve of force vs deflection is used to calculate the reduced (Indentation) Young's modulus (E^1) based the Hertz Sneddon model Equation 1 (Sneddon, 1965):

$$F = \frac{4}{3} E^1 \sqrt{R\,(d - d_0)^2} \tag{1}$$

where R is tip radius, F is force applied and $d - d_0$ is the displacement.

Each measurement of load/displacement was made in 6ms. Further information on the QI ™ is avaliable in "QI™ mode-quantitative imaging with the NanoWizard 3 AFM" (Instruments, 2011).

The AFM QI™ was first calibrated in non-contact mode; a method suggested in the JPK documentation (Instruments, 2011). In this method the cantilever is flexed, whilst measuring the movement of lazer from the deflection of the tip, the movement of the tip is known from the spring constant of the cantilever, and this allows calibration of the photo-diode sensitivity. Further calibration is undertaken a by scanning a standard of Highly Ordered Pyrolysed Graphite, with a known modulus of 18GPa. The sensitivity and spring constant were then adjusted to give a reading within a standard deviation of 18GPa.

AFM QI™ scans were generally 512×512 pixels on an area of $250\,\mu m^2$. A minimum of four scans were undertaken per cutinite and sporinite maceral, which were generally on adjacent areas to give a representative overall distribution of each maceral, with two macerals (eight scans) scanned per coal sample. A total of twelve inertinite scans were obtained across the three coals - four scans per coal. Due to the larger particle size of the inertinite ($>250\,\mu m^2$), a minimum of two not necessarily adjacent scans were collected on each inertinite maceral, giving a total of six inertinite macerals analysed. For the same reason as inertinite, a minimum of two scans were obtained on the bituminite and cutinite within the Northumberland coal. Measuring Poisson's ratio of coal macerals at this length scale proves challenging, and as such all Young's modulus values are reported in Reduced modulus (E^1), which is also the case for values obtained from nanoindentation where Poisson's ratio is unavailable.

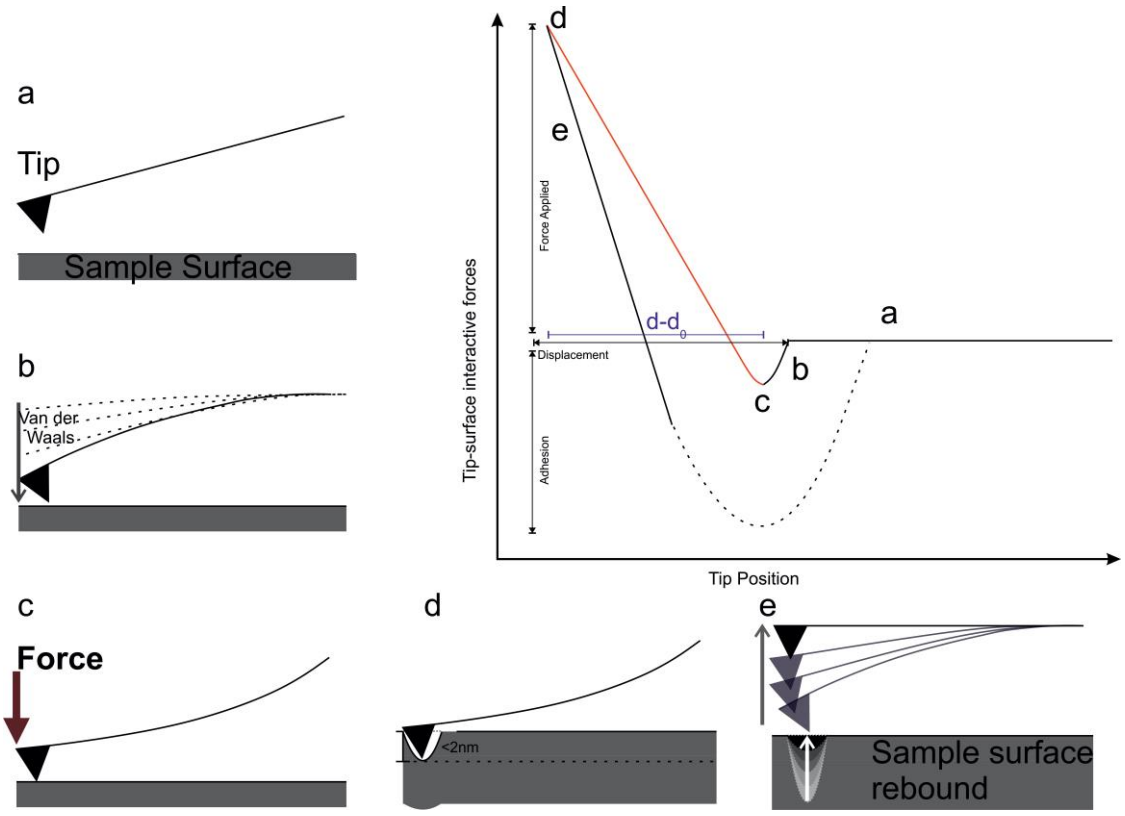

Figure 2: A graphical indication of the process of acquiring an AFM measurement. Initially the tip starts away from the sample surface (a), once the tip is brought towards the surface of the sample Van Der Waals forces adhere the tip to the surface (b), at the point of maximum adhesion (c) a force is exerted onto the sample surface, until at a point (d) the preset maximum force is exerted. At this point (d) the tip is allowed to leave the sample surface. The reduced Young's modulus is calculated along the extend curve (red) using the Hertz-Sneddon equation (Equation 1).

2.4. Mercury Injection Porosimetry

Pore size distribution and total porosity analysis was undertaken on the samples of coal only using Mercury injection. This analysis wasn't undertaken on the New Albany Shale due to the difference in porosity associated with bulk shale and isolated kerogen. The mercury injection was undertaken at Aberdeen University, using a Micrometrics Autopore IV 9500. The maximum injection was 30kPa corresponding to 3.7nm. Samples of $\sim$ 2.5cm^3 were selected. The data reported here are the mean pore diameter from intrustion.

3. Results and Discussion

3.1. Coal and Maceral Petrography

In total twelve individual macerals have been scanned using AFM QI ^{TM}for this study from three different coals and one shale. These roughly fit into seven seperate categories of maceral; immature sporinite, immature cutinite, immature alginite, mature cutininte, mature bituminite and inertinite (from immature and mature coals).

The sporinite within the Cannel coal (Figure 3c,d) is the finest grained of any of the macerals existing as fluorescing doubled over structures approximately 10-50μm along axis, which either exist in clumps or more occasionally as individual spores. The spores are in general relatively well-preserved. The inertinite within the Cannel coal is very coarse grained compared to the other macerals present (Figure 3i,j), appearing generally as laminated blocks up to 500μm along axis parallel bedding.

The macerals within the Paper coal are generally larger than the aforementioned Cannel. For example the cutinite within the Paper coal appear as 100-400μm long and approximately 10-20μm thick laminae which are readily distinguishable under ultra violet light (Figure 3a,b). Similar to the sporinite these liptinite macerals show little evidence for oxidation. The inertinite within the Paper appears as a relatively minor constituent and similar to the Cannel coal, appears as large blocks with relatively small amounts of inertinite within the matrix of the coal.

In contrast, the Northumberland coal has a very different appearance to the other two coals studied; richer in vitrinite and inertinite, indicative of a more oxidising depositional environment. The bituminite in the Northumberland coal appears as millimetre long bands oriented parallel to bedding and has a low fluorescence under UV light. The occasional Sporinite macerals in the Northumberland coal are slightly oxidised and broken with a low fluoresence. Cutinite macerals within this coal appear as the most fluorescent component but are much smaller than the equivalent in the Paper coal. The abundant inertinite within this coal appears as large bands similar to the other coals but also within the coal matrix (Figure 3f).

3.2. Vitrinite Reflectance

Vitrinite reflectance analysis of these coals confirms the difference in maturity identified by the difference in fluorescence of the liptinite macerals. Analysis suggests that The Cannel and Paper coals are 0.38% and

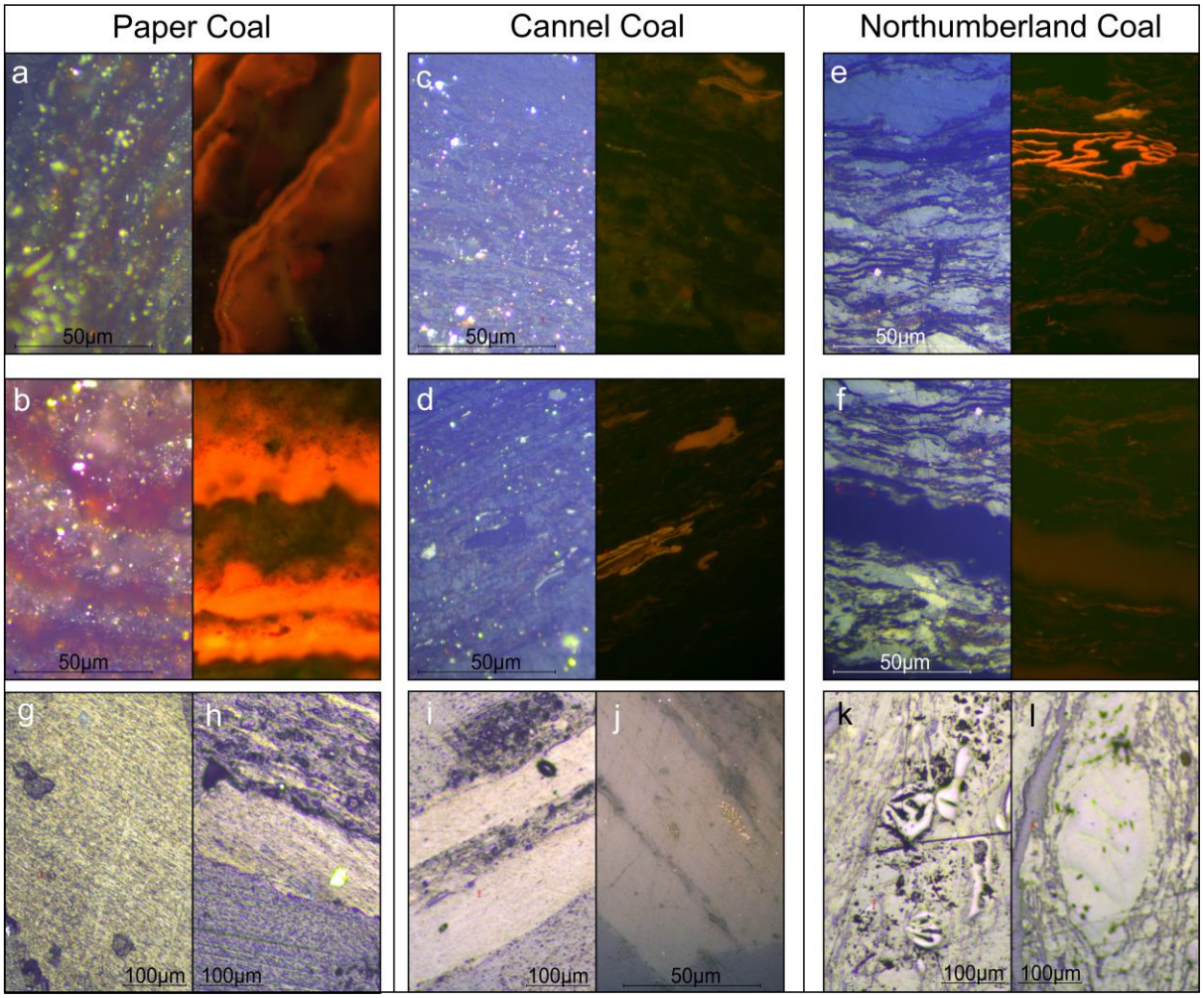

Figure 3: Photographs of the Coal macerals studied. Photos show cutinite (a,b,e), sporinite (c,d), bituminite (f) and inertinite (g-l). The left column are from the Paper coal, the middle column from the Cannel coal and right column from the Northumberland coal.

0.39%R_o respectively with the Northumberland coal being significantly more mature at 1.56%R_o. Maturity analysis wasn't undertaken on the New Albany Shale, though results from other studies on samples from the same location suggest an approximate R_o of 0.65% (Mastalerz et al., 2016).

3.3. Young's Modulus of Coal Macerals

The kernel density estimates and the mean and modal values of Young's modulus for alginite, sporinite, cutinite, bituminite and inertinite from mature and immature coals are shown in Figure 5. The mean and modal Young's modulus values of the macerals studied are also given in Table 2. Due to the resolution of each measurement (~10nm), we believe that this reflects a true local modulus of an individual phase rather than the effective modulus obtained from nanoindentation. In total alginite, sporinite, cutinite and bituminite macerals have been analysed from the liptinite group along with three different types of inertinite macerals.

3.3.1. Liptinite Macerals

The alginite in the New Albany Shale is tri-modally distributed, with peaks at ~ 2.5, 4.5 and 5.5GPa. The reason for this trimodal distribution is likely a reflection of the limits of polishing a kerogen isolate in terms of the smoothness required for AFM. This makes it difficult to adequately differentiate between the alginite scanned (E=3-7GPa) and the resin in which the particles of alginite are set. AFM analysis of the resin indicates a modal modulus value of ~5.0GPa. There appears to be very limited research undertaking AFM on isolated kerogen; which may be due to the preparation and mounting method for kerogen isolation not being optimal for AFM analysis. Therefore the alginite values described here shall be disregarded.

The two sporinite rich areas scanned in the cannel Coal have the lowest modal and mean Young's modulus values of the macerals studied, with modes of 1.1GPa and 1.74GPa, and means of 3.51GPa and 2.86GPa (Figure 5a). The modal value within the sporinite rich scans also has the highest probability frequency (~ 0.245). The cutinite rich scans in the Paper coal have the highest mean modulus values of all macerals studied (8.83GPa and 9.10GPa) (Figure 5b)., and the largest difference between these aforementioned mean values, and the equivalent modal value (3.78GPa, and 2.19GPa). The comparably thermally mature cutinite has a similar mean modulus (8.43GPa), which is the third highest modulus studied, but with a mode of 6.99GPa (Figure 5d)., which is closer to the mean than in the immature equivalent. The modal value of bituminite is 6.27GPa and a mean of 7.11GPa. This is the second highest modal value within the macerals measured (Figure5d).

There is a clear trend in reduced Young's modulus distribution within the liptinite macerals sampled; with immature macerals being less stiff than their mature counterparts. There is also a generally larger difference between the mean and modal values of E^1 in the immature sporinite and cutinite macerals, which is indicative of a non-normal distribution (Table 2).

When comparing the frequency of the distributions of immature macerals it is obvious that the sporinite measured is incredibly homogeneous. In contrast the cutinite has a large degree of heterogeneity, indicated in the difference in modal frequencies in Figure 5 and appearance in Figure 4. It may be that sporinite is more homogeneous than cutinite in general, indicative of the mechano-chemical compositional differences. Another possibility for the difference is the size of the macerals. As already noted the macerals of cutinite in the paper coal are larger than the sporinite in the cannel coal (Figure 3a,b vs Figure 3c,d), which may allow for measurement of more internal heterogeneity within the cutinite, causing a more varied modulus distribution. Another possible explanation for this difference is the interaction between mineral matter/groundmass and the cutinite macerals in the form of mechanical layering. There appears to be relatively little mineral matter (E^1 > 15GPa) in the vicinity of the sporinite measured in comparison to the different colours and larger portions of masked out modulus in the immature cutinite scans (Figure 4). This would cause a spread distribution in the cutinite, as many measurements would be made of cutinite/mineral matter contributing to a higher mean modulus value and a lower frequency of the modal modulus.

There is clear evidence for a transition in modulus mode and mean values of liptinite macerals with

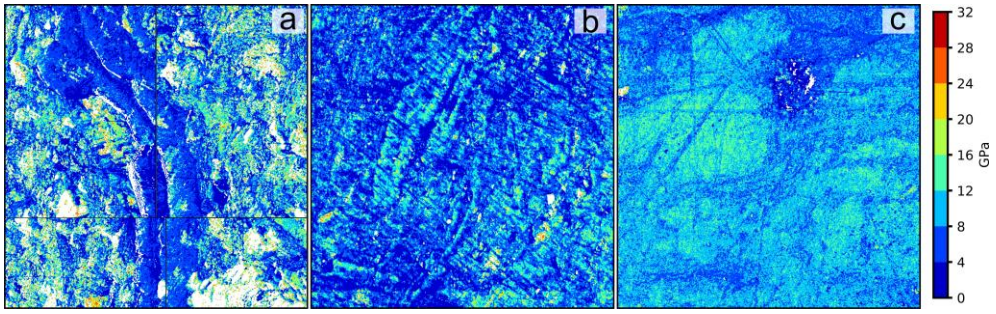

Figure 4: A selection of AFM Young's modulus scans including (a) immature cutininte from the Paper coal, (b) immature sporinite from the Cannel coal and (c) mature cutinite from the Northumberland Coal. Areas of white in the scans are places where the reduced Young's modulus is greater than 30GPa. It is obvious from both these scans and Figure 5 that there is far more heterogeneity associated with immature cutinite (a) than either the immature sporinite (b) or mature cutinite (c). ^{I} denotes from an immature coal, whilst ^{M} denotes from a mature coal.

maturity. The bituminite and cutinite from the Northumberland coal have a modal value between twice and five times greater than the immature sporinite and cutinite. These modal values are also similar to the mean value, suggesting a more gaussian distribution. This most likely reflects a transition in mechanical properties related to chemical changes in the macerals with maturity. Hydrogen rich macerals are known to lose a lot of aliphatic and Nitrogen, Sulphur and Oxygen rich Hydrocarbon compounds in the oil window and become aromatic dominant by the gas window (Pan et al., 2013), which may be reflected in the stiffer, more normal distribution exhibited by the Northumberland liptinite.

3.3.2. Inertinite

The inertinite in the cannel coal show two distributions, which are not observed between two different scans in any of the other macerals. One piece of inertinite has a mode and mean similar to the sporinite (mode: 1.23GPa, mean: 2.36GPa) (Figure 5a). The second distribution, however, is almost twice as stiff and unlike any of the other immature distributions is approximately normally distributed with a mode of 3.69GPa and a mean of 3.60GPa.

The modal (2.49GPa and 3.72GPa) and mean values (4.05GPa and 4.92GPa) for the inertinite within the paper coal are similar too, albeit slightly stiffer than that observed within the more normally distributed cannel (Figure 5c). The reduced Young's modulus values of the inertinites canned from the mature Northumberland coal are larger than the immature equivalent with a modal value of 4.59 and mean of 5.87GPa. The distribution of the mature inertinite appears to be almost normal, although with a limb between 0 -1.5GPa, where values of modulus in this range are relatively infrequent. This limb appears in a similar region to the modal value of the Cannel Coal inertinite, which may be indicative of a transformation from immature inertinite to another more mature form or from the loss of this mechanical element during primary oxidation, which formed the inertinite.

A trend of slightly higher modal values of modulus in the inertinite macerals measured within the imma-

Coal	Maceral	Mode (GPa)		Mean (GPa)
		AFM	5μm distribution	
Immature				
New Albany Shale	Alginite	2.91*	3.09*	6.19*
Paper Coal	Cutinite	2.97	9.76	9.27
Cannel and Paper Coals	Inertinite	3.21	3.81	3.72
Cannel Coal	Sporinite	1.35	2.85	3.19
Mature				
Northumberland Coal	Bituminite	6.27	6.79	7.11
	Inertinite	4.59	4.62	5.91
	Cutinite	6.99	7.81	8.43

Table 2: Modal an mean values of AFM QI^{TM}on each coal maceral. *Values of Alginite are affected by the interaction of the alginite/tip with the resin.

ture cannel coal than the equivalent inertinite in the Paper coal most likely represents regular heterogeneities exhibited between coals of similar maturity, but with different burial histories and associated stress fields. It is unclear as to why these two inertinite macerals have different properties but is most likely a result of; 1) differences in the type of inertinite (i.e. different source organic matter), 2) different amounts of oxidation prior to burial or 3) differences in the orientation of the maceral regarding any internal structure.

3.3.3. Trends in Modulus Values

The most obvious trend in Young's modulus of coal macerals is the aforementioned evolution with maturity, whereby macerals appear to become stiffer, more normally distributed and more heterogeneous. Figure 5 demonstrates this trend, with the mode and mean values generally increasing and becoming less separated with maturity. The frequency of the mode also appears to generally decrease with maturity, indicating that in general the macerals are becoming more mechanically heterogeneous. The exception to this is the immature cutinite macerals, which have the highest mean modulus and lowest frequency mode. These macerals are as mentioned previously influenced by mineral/groundmass which is stiffer than the maceral itself.

A notable trend is the amount of stiffening in the liptinite macerals relative to the inertinite macerals with maturity. The liptinite macerals modal moduli increases by a factor of between two and five with maturity, whereas the modal value for inertinite only increases by approximately 42% (Figure 5c., Table 2). The modal value of inertinite increased by 1.17GPa from the Paper coal to the Northumberland coal, whereas the cutinite increased by 4.02GPa between the same two coals. This trend indicates that thermal maturity is almost certainly the main drive in the transition of modulus values and distribution. The inertinite which is most likely thermally matured or oxidised at surface is less effected than the hydrogen rich liptinite macerals. This may therefore only represent the mechanical 'maturation' with increased burial depth. This change in

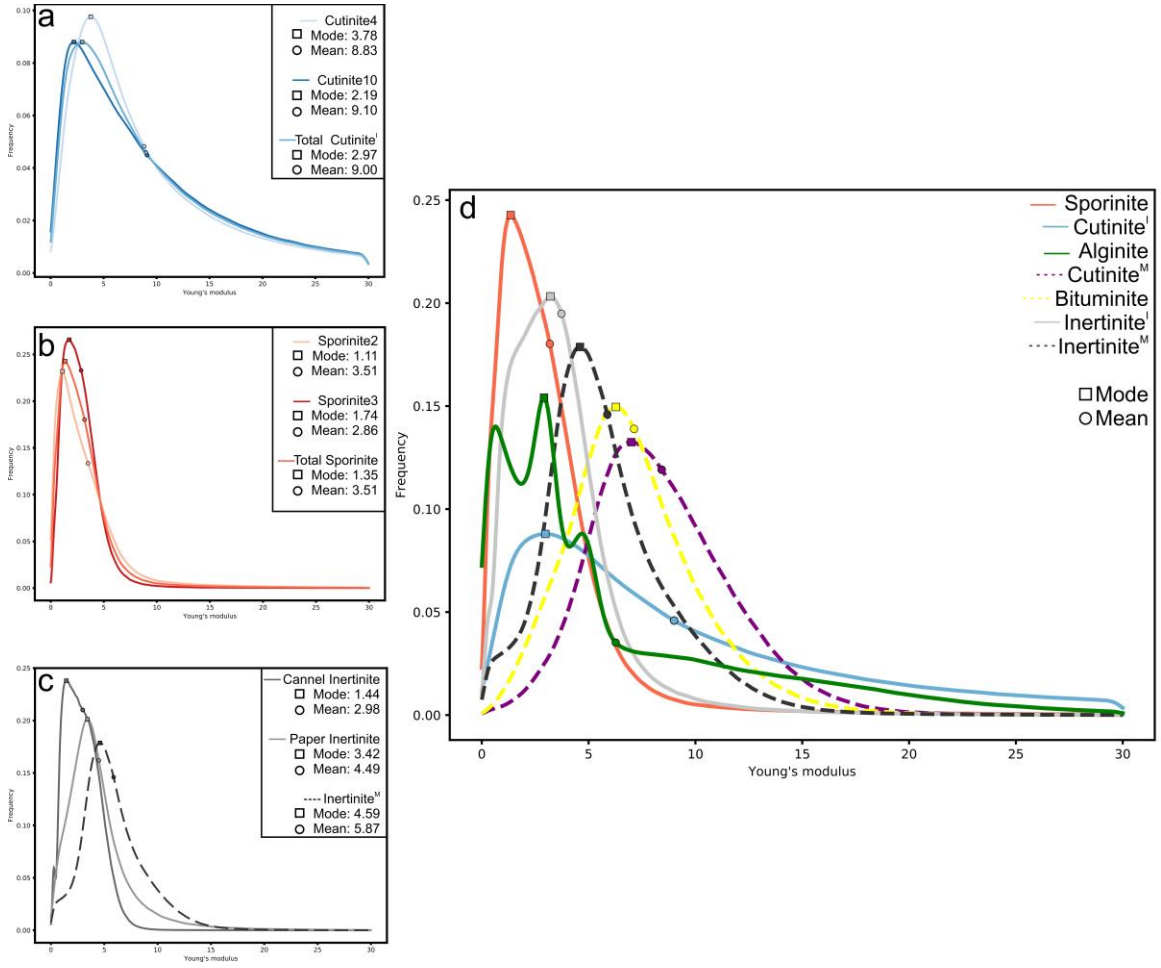

Figure 5: Probability distributions of each of the macerals studied, (a) is the distributions of immature cutinite from the Paper coal, (b) is the distributions of immature sporinite form the Cannel coal, (c) is the distributions of inertinite in all three coals and (d) is a composite chart of all macerals studied. Block lines are from immature coals (Paper and Cannel), dashed lines are from the Northumberland Coal. Boxes indicate the modal value of each distribution, circles are the locations of the mean values from each distribution. In the immature shales the liptinite macerals have a lower modulus than their inertinite counterpart, a relationship which inverts with maturity. Liptinite macerals increase in stiffness drastically with maturity, as well as becoming more Normally distributed. Inertinite also becomes stiffer with maturity, although to a lesser extent than liptinite, which may be due to the oxidized state in which the inertinite was deposited. n.b. ^{I} denotes immature macerals, ^{M} denotes mature macerals.

Coal	Porosity (%)	Mean Throat Diameter (nm)
Cannel	3.19	6.34
Paper	7.45	16.83
Northumberland	9.88	7.39

Table 3: Mercury injection porosimetry derived total porosity and mean pore radius size values for each coal.

liptinite macerals may be associated with the transition in chemistry from chaotic to an ordered aromatic structure (Pan et al., 2013) along with the same mechanical maturation associated with the inertinites.

It appears from the results obtained here that the macerals analysed show a larger variability than in previous AFM literature on coals (Li et al., 2020), and are in general significantly less stiff. The modulus results obtained are closer to those found within nanoindentation literature (Kossovich et al., 2016; Zhang et al., 2018b,a; Borodich et al., 2015). However, it is not prudent to directly compare effective reduced Young's modulus with local reduced Young's modulus. The reasons for this are linked to both internal porosity at length scales between the AFM and nanoindentation measurements (Table 3). This porosity would certainly decrease the effective modulus, but would not affect the AFM measured local modulus. Another reason for caution in comparing AFM and nanoindentation is the effect of the central limit theorem, which indicates that the collection of means of any distribution are normally distributed (Bauer, 2011). As the nanoindenter measures the mean modulus at a length scale of $\sim 25\mu m^2$ any collection of nanoindentation curves should be normally distributed. However, the actual modulus of each component, measured by AFM may be entirely non-normally distributed. A further analysis of this to attempt to contrast AFM and nanoindentation is undertaken in Section 3.5.

When analysing for the CCUS potential of a coal it is common to undertake a point count analysis for the maceral content of the coal chosen. Despite this a key method to estimate the effects of CO_2 injection on the physical properties of coals is models derived from laboratory based experiments. These models take the coal modulus as a whole but any maceral variability is not accounted for. All modelling attempting to represent swelling from injection pressure of CO_2 uses Young's modulus of the coal medium as a key input (Pan and Connell, 2007; Zhang et al., 2008; Connell and Detournay, 2009; Liu et al., 2010; Ma et al., 2011; Liu et al., 2019). However, the variability exhibited within the macerals analysed is of even greater importance. The highest modal value of Young's modulus is more than 500% of the lowest modal value. This is between two liptinite moduli (sporinite and mature cutinite), suggesting that just knowing the proportion of liptinite/inertinite/vitrinite/mineral isn't enough, the coals must be analysed for precursor material.

3.4. Organic Matter Distribution Analysis

As mentioned a key feature of each maceral Young's modulus is the distribution shape. This is reflected as a transition to a more normally distribution with maturity, shown by a smaller proportional gap between modal and mean values of Young's modulus. Previous studies use homogenisation of nanoindentation results

to estimate the Young's modulus and hardness values for minerals within rock (Bobko and Ulm, 2008; Ulm et al., 2007; Ulm and Abousleiman, 2006; Liu et al., 2018; Li et al., 2019). This technique is a form of modelling, whereby the distribution of the nanoindenation results is a composite of normal distributions for each phase multiplied by its respective proportion in the rock indented. Deconvolution is successful due to the central limit theorem mentioned previously, as the mean of the nanoindentation moduli will always be normal even if the distributions themselves are not. Deconvolution also works best for phases whose mean distributions across this length scale show a relatively small variation and aren't mechanically coupled with other phases, therefore producing a sharp noticeable normally distributed peak (Calcite, quartz, pyrite etc.). However, at higher resolutions or with increased testing, this technique may not be ideally suited as some distributions trend toward the non-normal. In the coals and shale studied here the distribution of the organic matter appears to be non-normal. As such it is important to identify which distribution may be more appropriate to add to the deconvolution model for organic matter.

In order to facilitate this, each maceral has been analysed against a set of distributions (Normal, Log-normal, Gamma) to minimize the error between the proposed distribution and the observed distribution (Equation 3). The minimization was carried out initially a by the python based scipy.fit program for each of the distributions shown. The fitted parameters were then used as an initial guess to undertake a single phase deconvolution, using a method similar to that presented in Bobko and Ulm (2008). The N observa- tions are sorted and the Experimental Cumulative Density Function(ECDF) is then formed by the F_M of these N points using Equation 2. The ECDF is then minimized for root mean square error against a CDF generated the fitting parameters of each of the three distributions in order to obtain the minimum error (Equation 3). The minimization was undertaken using scipy optimize least squares package, which uses the Levenberg-Marquardt Algorithm, for information on this package readers are directed to lea & More (1977).

$$F_M(M_i) = \frac{i}{N} - \frac{1}{2N} \quad \text{for i} \in [1;\mathrm{N}] \tag{2}$$

$$\begin{aligned} \min\left[(\mathrm{CDF}(\mathrm{X} \sim \mathrm{N}(\mu, \sigma)) - \mathrm{ECDF})^2\right] \\ \min\left[(\mathrm{CDF}(\mathrm{X} \sim \Gamma(\mathrm{k}, \theta)) - \mathrm{ECDF})^2\right] \\ \min\left[(\mathrm{CDF}(\mathrm{X} \sim \mathrm{LogNorm}(\mu, \sigma)) - \mathrm{ECDF})^2\right] \\ \text{Where}: \mu > 0.0 \end{aligned} \tag{3}$$

The results of the minimization are shown in Figure 6, which indicate that although no single distribution matches the maceral distribution absolutely. It appears that for sporinite, cutinite (immature and mature) and Northumberland inertinite the Gamma distribution appears to fit the most accurately. For the bituminite and inertinite from the immature coals the Normal distribution appears visually to fit as well as the Gamma distribution. The Normal distribution appears the best fit for Inertinite from the thermally immature Cannel and Paper coals. Although it should be noted that some of these distributions (mature cutinite, mature inertinite, bituminite) appear to be a mixture between Gamma and Normal distributions. The

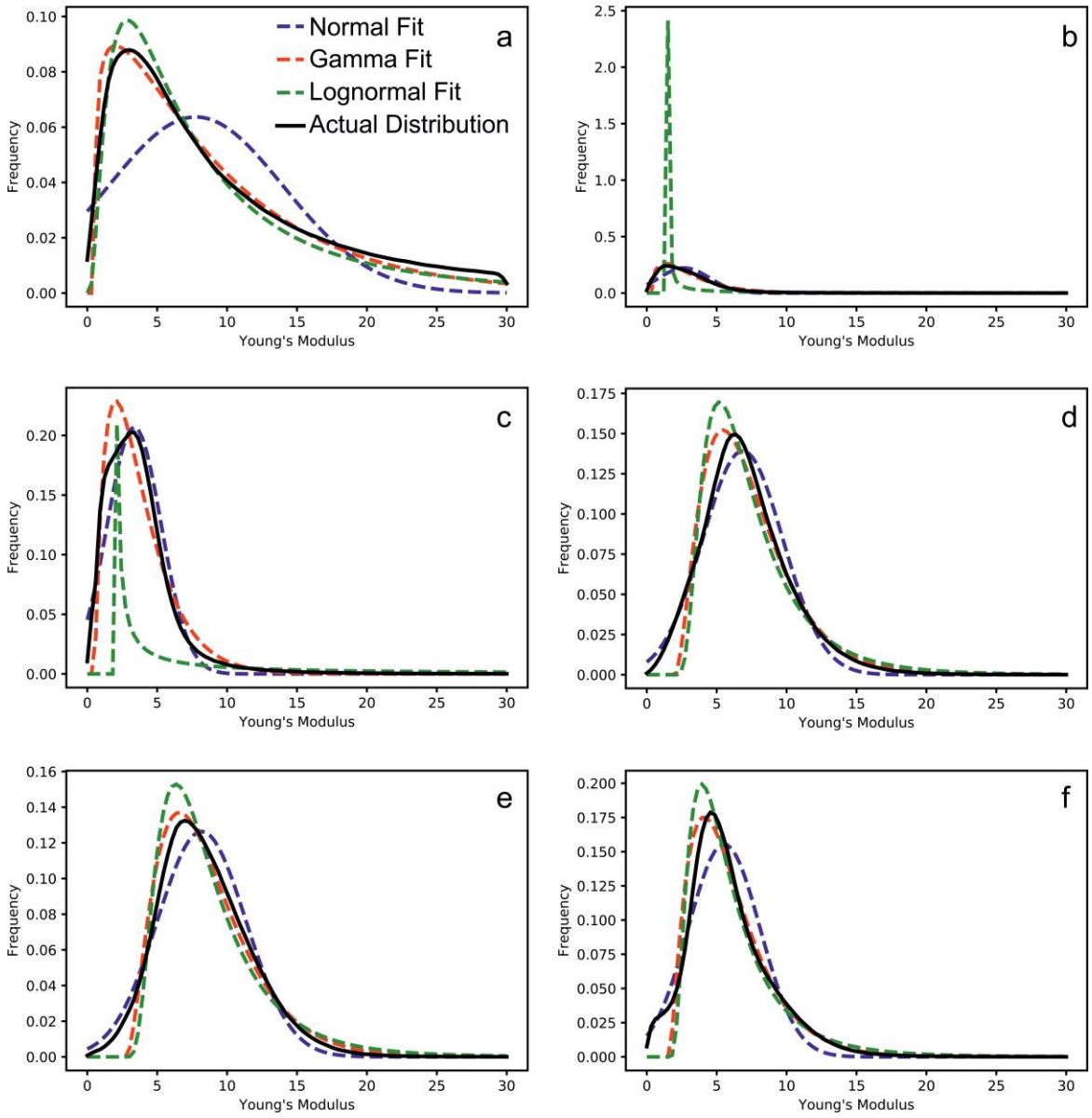

Figure 6: A comparison of the AFM distribution with the optimum Normal, Gamma and Lognormal Distribution for immature cutinite (a), sporinite (B), immature inertinite (c), Bituminite (d), mature Cutinite (e) and mature inertinite (f). The Gamma distribution appears to be the best fit for all macerals apart from immature inertinite. The Normal distribution is the next best fit visually aside from the immature cutinite distribution. The Lognormal distribution is the poorest fit for each distribution and is particularly poor for sporinite.

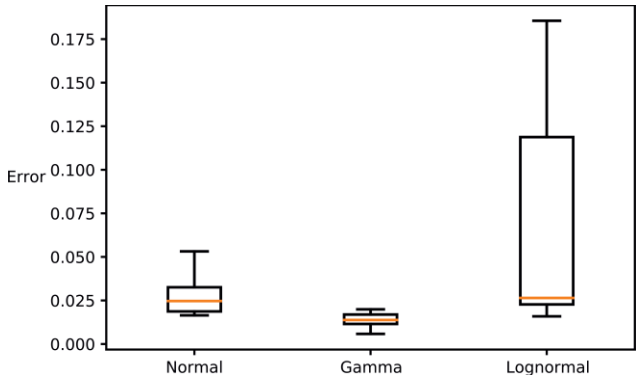

Figure 7: The error associated with each distribution. The Gamma distribution has a low error value for each maceral and a relatively small standard deviation in error. The Lognormal error is high, partly due to the poor fit on Sporinite. This error indicates that a Gamma distribution is most appropriate to generalise coal maceral Young's modulus data

Maceral	Normal Error	Gamma Error	Lognormal Error
Cutinite^{I}	0.053	0.006	0.015
Sporinite	0.034	0.011	0.149
Inertinite^{I}	0.022	0.020	0.186
Bituminite	0.016	0.018	0.028
Cutinite^{M}	0.018	0.013	0.024
Inertinite^{M}	0.027	0.014	0.022

Table 4: Root-Mean-Squared-Error for each distribution fit for each Maceral. ^{I} denotes from an immature coal, whilst ^{M} denotes from a mature coal

Lognormal distribution, although selected for this comparison due to its visual similarity to some of the maceral distributions performs poorest out of all the distributions. Further investigation indicates that the constraint of a positive mean (as negative mean Modulus is unrealistic) causes the Lognormal distribution to lose the fitting capacity for almost all the macerals.

Detailed analysis of Figures 6 &7 and Table 4 suggests that the normal distribution used for deconvolution is less appropriate for immature hydrogen rich macerals, with the highest error values associated with immature cutinite and sporinite (Figure 6a,b), which have twice the error of fit when compared to the mature liptinite macerals (Figure 6d,e). The Gamma distribution actually shows the opposite error trend, whereby the least fit error is associated with the immature cutinite and sporinite distributions 4

Figure 7 displays the error associated with fitting each distribution, which clearly demonstrates that the Gamma distribution is the most likely fit for the coal macerals analysed. This distribution has a maximum error below the mean error for the Normal distribution. These findings suggest that any homogenisation using coal macerals at this scale should be done using a Gamma distribution. This relationship may assist in attempts to upscale and homogenise coal Young's modulus measurements, which in turn may help assist injection models.

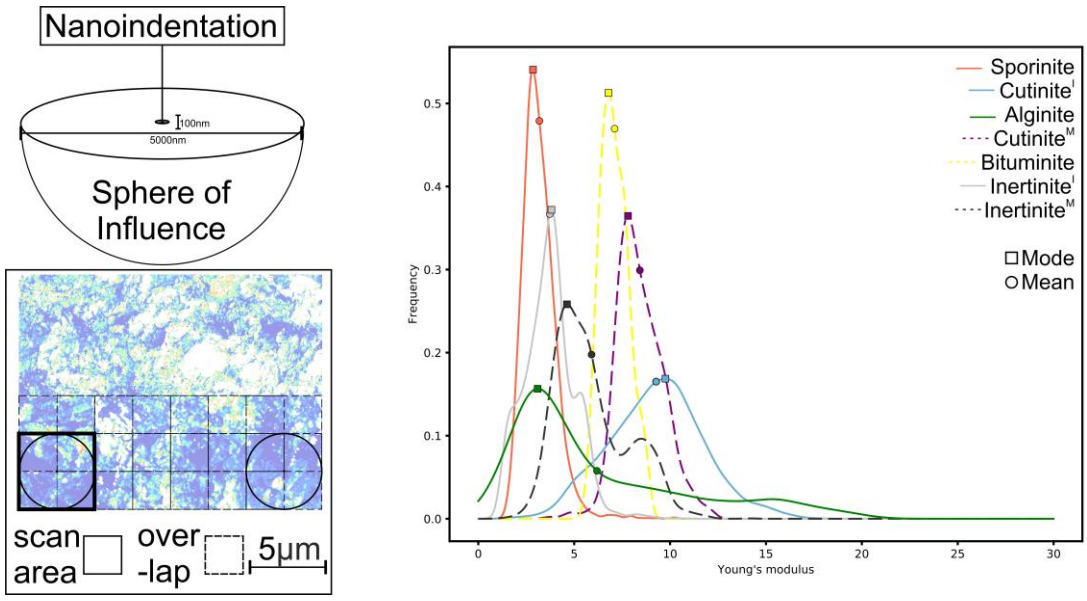

Figure 8: The distribution of mean values for AFM when analysed at $25\mu m^2$ increments. This gives a total of 361 mean measurements for each $50\mu m \times 50\mu m$ area. The left of the figure indicates the approximate area of influence for a nanoindentation scan 100nm deep, which is a hemisphere of radius $\sim 5\mu m$. The figure on the right indicates the probability distributions of the means. Each of the modal values are greater than those in the overall local AFM population (Figure 5), the modal value of the immature cutinite means is significantly greater than the local AFM distributions indicated in Table 2. n.b. ^{I} denotes immature macerals, ^{M} denotes mature macerals.

Results from the minimization indicate that the shape parameter a is in the range of 1.20 (immature cutinite) to 2.87 (mature cutinite). A scale parameter (θ) is required along with the shape parameter a to fit the Gamma distribution. The calculated values of θ range from 1.70 in immature inertinite to 7.26 in immature cutinite.

Furthermore shale organic matter should be analysed to identify if the Gamma distribution is a better fit for all organic matter. This may also inform as to whether a Normal distribution is most prudent for deconvolution of shales at higher resolutions than nanoindentation or if other distributions may offer greater accuracy.

3.5. Mean Analysis

In order to attempt a comparison between the AFM results reported here and the literature nanoindentation values the AFM scans were analysed to gather mean values across a $5\mu m \times 5\mu m$ area with a $2.5\mu m$ overlap with the adjacent means (dashed line in Figure 8). This upscaling gives a square of similar size to the 2D zone of influence of a nanoindent (Figure 8). These are reported in this literature as effective moduli values with the effective size of $5\mu m$.

Figure 8 displays the effective modulus distribution acquired from $5\mu m$ means for each set of macerals, indicating a distinct increase in modal value when compared to the overall distribution of each maceral. Table 2 indicates the modal values for each of the macerals in this format, mean values are the same as

the mean for the overall distributions. The increase in modal value from this technique is widest in the immature cutinite where the Young's modulus increases by more than 325% (2.97GPa to 9.76GPa). The smallest increase is ~ 0.5% within the mature inertinite. This increase with 5 μm averaging is greatest in macerals with the the highest degree of non-normality (Table 4). This absolute increase in coal Young's modulus with maturity has been indicated at higher length scales with UCS/uniaxial or triaxial compression tests by other studies (Pan et al., 2013; Morcote et al., 2010). The increase in modulus observed by AFM is greater than that observed in literature and may be a result of the decreased effect of the mineral proportion on the AFM modulus distribution. The mineral phase in these coals is unlikely evolve or stiffen with maturity to the same extent that the organic matter in coal does within the maturities measured here.

It is noted that these results more likely represent the appearance of macerals at higher length scales, which is indicated by Figure 8. This increase in modal modulus is to be expected considering the distributions will conform to the central limit theorem (Bauer, 2011). This is due to each of the distributions being most similar to a gamma distribution with a mean greater than the mode, which will combine to a normal distribution with a mode close to the mean of these distributions.

The effective modulus distributions are generally normally distributed with the exception of alginite, and inertinite. As mentioned previously there is significant interference between the alginite and the resin encapsulating it, which explains the bimodal distribution of the 5 μm distributions. It does however appear that there are more than one phase within both the mature and immature inertinite. This is particularly interesting as there is little to no groundmass in these scans due to the particle size of the inertinite. A primary reason for this also could be the difference between two individual macerals of inertinite, however, two individual macerals were scanned of both immature cutininte and sporinite and resulted in a normal distribution.

The effective modulus distributions of the mature coal fit closer to the distributions acquired by Li et al. (2020), which are at a similar length scales, albeit somewhat softer than the modulus values obtained in that study. Their study also implies that the average modulus of the 'mineral' content of a coal, most likely quartz, pyrite and clay minerals have an average Young's modulus <20GPa, which appears to be unlikely.

The effective modulus distributions of organic matter appear to be within the ranges of those stated within nanoindentation the literature (Yu et al., 2018; Zhang et al., 2018b, 2017) (Figure 9), although slightly lower than some values. The reason this could be; the difference in maturity between the samples analysed here and those in the aforementioned literature, or the influence of mineral inclusions which may bolster the effective Young's modulus at the length scale of nanoindenation, which are masked out in this form of AFM due to being stiffer than the tip used. If mineral matter were to be a major contributing factor, then the increased porosity measured at nanoindation would decrease modulus readings by similar amounts. Results of nanoindentation from Kossovich et al. (2016); Zhang et al. (2018b,a); Borodich et al. (2015) give modulus values of coal between 3-9GPa, which are within the ranges exhibited here (Figure 9), suggesting that this averaging technique may be applicable to upscale modulus values from AFM length scales to

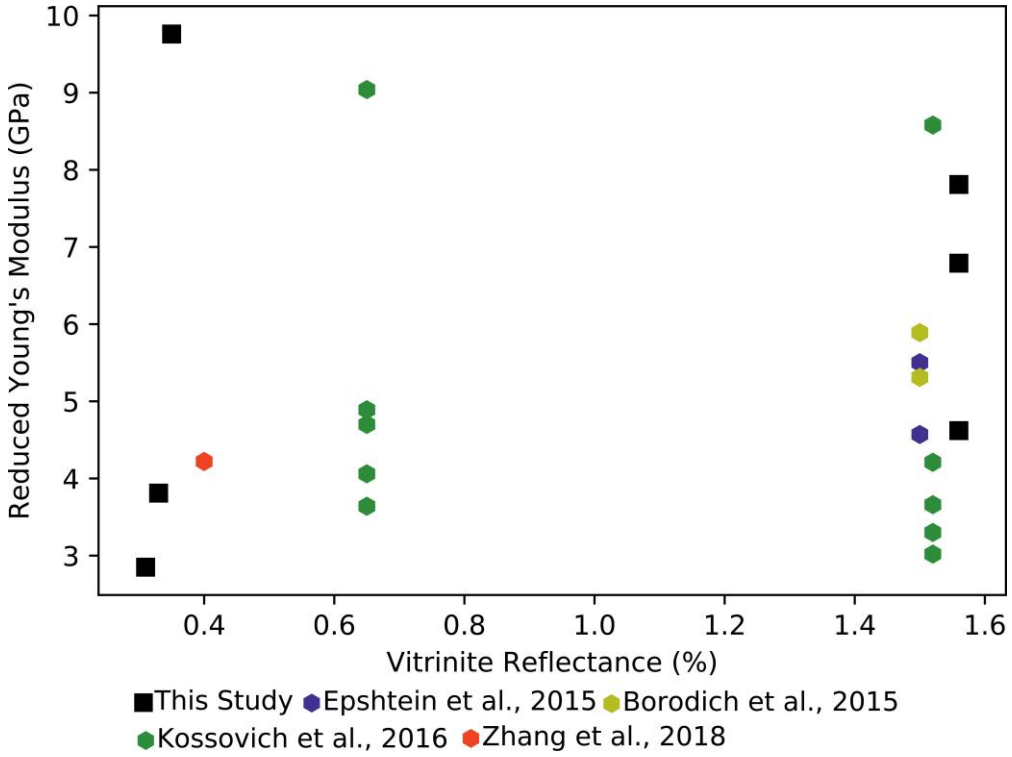

Figure 9: A comparison of the mean distributions of AFM from this paper with nanoindentation values from other literature, at the maturities measured. The means of the AFM distributions are within the range of literature values acquired from nanoindentation at the maturities measured. The mean of the immature cutinite may be marginally above the literature reported but is most likely due to the interaction with mineral matter/groundmass.

Nanoindentation length scales in simplistic three phase systems (maceral, porespace, mineral matter).

It is not always prudent to further upscale these AFM results to the region of triaxial experiments due to the formation of cleats and fractures within the coal, which are not analysed by the AFM. However, Gentzis et al. (2007) found static Young's moduli values of between 1.1-5.1GPa with no pore pressure and Poisson's ratios of between 0.26-0.48. The equivalent Young's moduli values of our maceral means when analysed with Poisson's ratios of 0.26 are 2.97-8.65GPa and with $\nu = 0.48$ are 2.45-7.14GPa, which although slightly stiffer than the triaxial values are not significantly different.

3.6. CO_2 *Injection Modelling*

The difference in modulus values within a single coal is crucial when investigating the deformation potential with regards to CO_2, as open phase fractures may readily form due to the differential swelling associated with different macerals. Figure 10 indicates the swelling associated from injection of gas using the Pan and Connell (2007) model of gas injection (Equation 4) and the standard inputs acquired by Levine (1996) (Table 5). The modal values of each distribution were chosen as the Young's modulus within this model. The simulation was undertaken using low pressure and a Langmuir adsorption isotherm, and assuming isotropic elastic behaviour.

Results of this modelling approach indicate that the linear strain exhibited in a maceral is directly linked to the Young's modulus, indicating that open fractures may occur between macerals of different moduli. These open fractures may either assist in the percolation of CO_2 through the coal during sequestration, or cause seepage into pre-existing fractures causing unwanted leakage. The increase in modal Young's modulus at higher length scales affect the strain associated with injection in immature macerals. In particular the strain associated with the local modal value of Cutinite three times greater than that if the cutinite is modelled from the effective modulus of 5 micron squares (Figure 10). This possible increased stiffening of coal at microscopic (nanoindentation) length scales may cause misinterpretation regarding strains from CO_2 injection.

Figure 5 indicates that the modal Young's modulus values increase in all macerals with maturity. This increase in modulus represents a decrease of approximately 30% in linear strain in the Pan and Connell (2007) model with maturity (Figure 10. The increase in liptinite maceral modulus is even more significant, with the modal values increasing from 1.35/2.97GPa in immature coals, to >6GPa in the bituminite and cutinite of the Northumberland coal. This represents strains 2-4 times greater than that observed in the immature sporinite and cutinite macerals compared to the mature bituminite and cutinite macerals under the Pan and Connell (2007) model.

$$E = \mathrm{RTL}\ln(1+\mathrm{BP})\frac{\rho_s}{E_s}f(x,\nu_s) - \frac{P}{E_s}(1-2\nu_s) \quad \text{Where:} \tag{4}$$

$$f(x,\nu_s) = \frac{[2(1-\nu_s)-(1+\nu_s)cx][3-5\nu_s-4(1-2\nu_s)cx]}{(3-5\nu_s)(2-3cx)}$$

The results of this modelling approach differ to the experimental approach undertaken by (Mastalerz et al., 2009) on the cannel and paper coals analysed within this paper. Mastalerz et al. (2009) indicate strains of between 0.42-1.05%. The differences in result are likely due to a combination of different length scales used: macerals in this study vs whole coals in Mastalerz et al. (2009), the need to update to macerals specific Langmuir inputs for the Pan and Connell (2007) model, and the higher maximum injection pressure in the experimental procedure than used in this study.

The overall outcome of injection modelling at a maceral scale further indicates the need to undertake detailed coal petrology prior to injection design. The juxtaposition of different macerals could either lead to opening of micro-fractures through differential swelling, enhancing permeability or expansion into the currently established fracture network, causing a net reduction in permeability. It is most likely that both will occur during injection, but the nanomechanical properties of the different macerals will cause these deformations to occur with different temporal and spatial resolutions. As the best outcome for injection into the subsurface is a predictable one, it is prudent to choose target strata that are thermally mature due to the limited variation between modal values of Young's modulus across different macerals, and their more normal distribution. This is further reflected in the similarity of the proportional strain exhibited by these

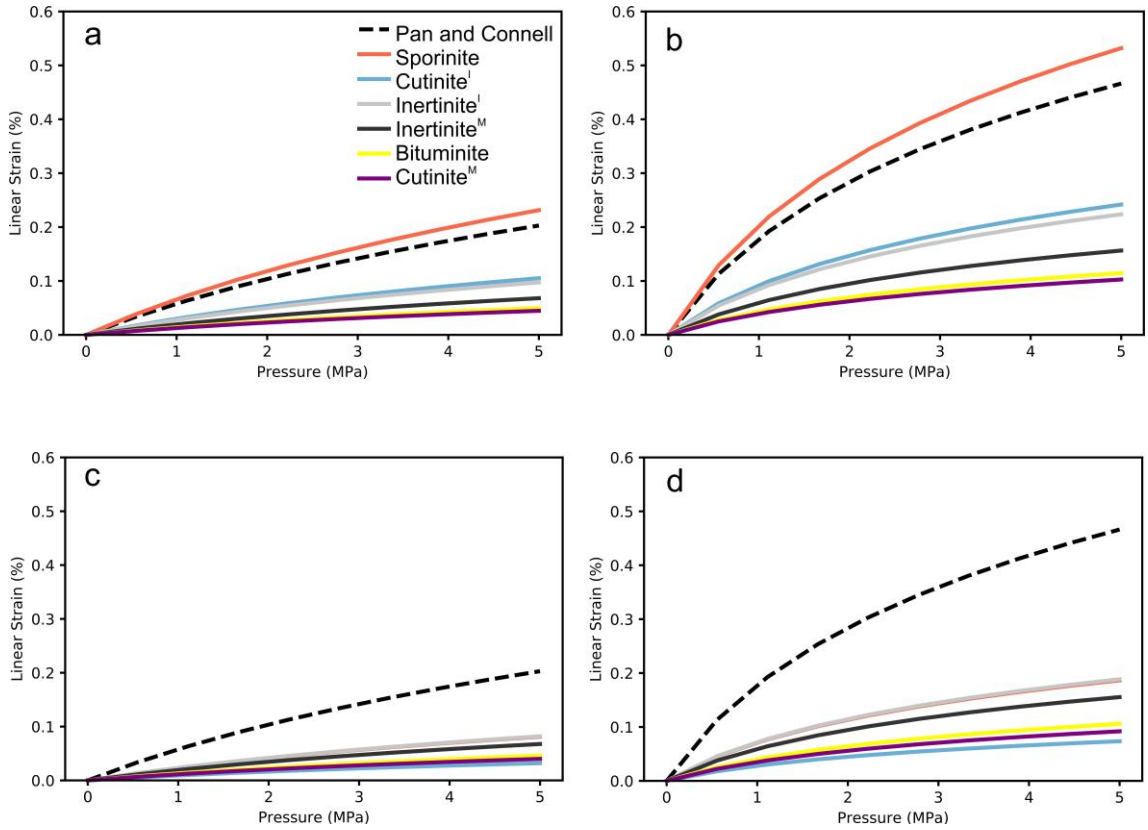

Figure 10: Gas injection pressure comparison with linear strain generated on each of the coal macerals using the Pan and Connell (2007) model and data from Table 5. The modal value of modulus was used to compute the results The strain related to each maceral from CH_4 (a), CO_2 (b) indicates that a lower Young's modulus causes greater linear strain upon injection. (c) and (d) are CH_4 and CO_2 injection into the macerals defined by their effective Young's modulus modal values (Table 2) from the 5μm mean analysis.

Symbol	Value	Description	Symbol	Value	Description
T	295(K)	Temperature	ρ	1.3(gcm^{-3})	Coal Density
R	8.314(J $mol^{-1}K^{-1}$)	Ideal Gas Constant	E_s	Table 2 (GPa)	Coal Young's modulus
L	1.257,1.488 ($molkg^{-1}$)	Langmuir Constanst	x	0.5	Diameter to length ratio of coal sample
B	0.294,0.953 (Pa^{-1})		c	1.2	Pore structure model constant
P	0-5(MPa)	Injection Pressure	ν_s	0.372	Coal Poisson's Ratio

Table 5: The inputs used for the Pan and Connell (2007) model for equation 4 taken from Pan and Connell (2007); Levine (1996)

macerals in Figure 10.

4. Conclusions

Cutinite, sporinite, bituminite and inertinite macerals were analysed for reduced Young's moudlus using Atomic Force Microscopy. Cutinte, sporinite were tested from immature Paper (0.31%R_o) and Cannel (0.35%R_o) coals originating from Kentucky and Indiana. Kerogen containing abundant alginite was analysed from the early thermally mature New Albany Shale (0.65%R_o). A thermally mature (1.56%R_o) coal from the Northumberland coalfield containing cutinite, bituminite and inertinite was also analysed.

The reduced Young's modulus of the liptinite and inertinite macerals are less than 10GPa, and are found to be non-normally distributed. The liptinite macerals from immature coals have the lowest reduced Young's modulus, with modal values between 1.4 – 3.0GPa. The equivalent inertinites in each coal have a modal modulus of (1.4 – 3.4GPa). The Young's modulus of alginite appears to be influenced by the encapsulating resin in which a kerogen isolate slide is traditionally mounted. It appears that kerogen isolation is an unsuitable technique to prepare samples for AFM testing. There is a general trend of stiffening with maturity in all macerals. However, this is greatly exaggerated in the hydrogen rich macerals. The modal modulus value of cutinite increases by 135%, in comparison inertinite only increases by 40%;

Analysis of the modulus distributions acquired from each maceral show a degree of non-normality. The immature liptinite macerals are the least normally distributed, with the mature liptinite macerals being the most normally distributed. Distribution matching indicates that a Gamma distribution is the most likely fit

for organic matter local Young's modulus in coals. This advancement allows classical deconvolution models to be adapted to account for these different length scales.

When upscaling local Young's modulus values to a 25 μm^2 area indicate a significant increase in Young's modulus is observed due to the inherent shape of the Gamma distribution, causing the mean value to be greater than the modal value in all macerals. The modal values across each maceral after this homogenisation process range between 2.9GPa in immature sporinite to 9.8GPa in immature cutinite. These values fall within the range of previously observed Young's modulus values of nanoindenation on coal. Therefore this simple homogenisation model represents an effective method of upscaling in mechanically homogeneous systems with only three main phases (maceral organics, mineral matter, porosity).

The modal Young's modulus values obtained in this study have been applied to the numerical Pan and Connell (2007) model, with all other attributes remaining standard from Levine (1996). This modelling approach indicates a direct inverse relationship between reduced Young's modulus and adsorption related strain. As such the maturity related relationships mentioned previously are also inverse to strain, whereby an immature maceral is likely to swell more than a mature maceral. Swelling of the macerals can either enhance porosity by creating open microfractures where macerals strain relative to the mineral groundmass, or reduce porosity by filling of cleats and existing fractures within the coal decreasing overall permeability. At higher maturities the difference in strain between inertinite macerals and liptinite macerals is less pronounced. Homogeneous mature coals therefore require much less sophistication when modelling, than a system with many differentially swelling components, and most likely reflect a more favourable CCUS target.

References

, . Scipy.optimize.least_squares documentation. . Accessed: 16-01-2020.

Alexeev, A., Revva, V., Alyshev, N., Zhitlyonok, D., 2004. True triaxial loading apparatus and its application to coal outburst prediction. International Journal of Coal Geology 58, 245–250.

Bauer, H., 2011. Measure and integration theory. volume 26. Walter de Gruyter.

Bickle, M.J., 2009. Geological carbon storage. Nature Geoscience 2, 815–818.

Bobko, C., Ulm, F.J., 2008. The nano-mechanical morphology of shale. Mechanics of Materials 40, 318–337.

Borodich, F.M., Bull, S., Epshtein, S., 2015. Nanoindentation in studying mechanical properties of heterogeneous materials. Journal of Mining Science 51, 470–476.

Bullock, L.A., Parnell, J., Perez, M., Armstrong, J.G., Feldmann, J., Boyce, A.J., 2018. High selenium in the carboniferous coal measures of northumberland, north east england. International Journal of Coal Geology 195, 61–74.

Cavanagh, A., Ringrose, P., 2014. Improving oil recovery and enabling ccs: a comparison of offshore gas-recycling in europe to ccus in north america. Energy Procedia 63, 7677–7684.

Connell, L., Detournay, C., 2009. Coupled flow and geomechanical processes during enhanced coal seam methane recovery through co2 sequestration. International Journal of Coal Geology 77, 222–233.

DiMichele, W.A., Rischbieter, M.O., Eggert, D.L., Gastaldo, R.A., 1984. Stem and leaf cuticle of karinopteris: source of cuticles from the indiana "paper" coal. American Journal of Botany 71, 626–637.

Eliyahu, M., Emmanuel, S., Day-Stirrat, R.J., Macaulay, C.I., 2015. Mechanical properties of organic matter in shales mapped at the nanometer scale. Marine and Petroleum Geology 59, 294–304.

Emmanuel, S., Eliyahu, M., Day-Stirrat, R.J., Hofmann, R., Macaulay, C.I., 2016. Impact of thermal maturation on nano-scale elastic properties of organic matter in shales. Marine and Petroleum Geology 70, 175–184.

Epshtein, S.A., Borodich, F.M., Bull, S.J., 2015. Evaluation of elastic modulus and hardness of highly inhomogeneous materials by nanoindentation. Applied Physics A 119, 325–335.

Espinoza, D.N., Pereira, J.M., Vandamme, M., Dangla, P., Vidal-Gilbert, S., 2015. Desorption-induced shear failure of coal bed seams during gas depletion. International Journal of Coal Geology 137, 142–151.

Gentzis, T., 2000. Subsurface sequestration of carbon dioxide—an overview from an alberta (canada) perspective. International Journal of Coal Geology 43, 287–305.

Gentzis, T., Deisman, N., Chalaturnyk, R.J., 2007. Geomechanical properties and permeability of coals from the foothills and mountain regions of western canada. International Journal of Coal Geology 69, 153–164.

Goodarzi, M., Rouainia, M., Aplin, A., Cubillas, P., de Block, M., 2017. Predicting the elastic response of organic-rich shale using nanoscale measurements and homogenisation methods. Geophysical prospecting 65, 1597–1614.

Hower, J.C., Trinkle, E.J., Raione, R.P., 2008. Vickers microhardness of telovitrinite and pseudovitrinite from high volatile bituminous kentucky coals. International Journal of Coal Geology 75, 76–80.

Ingram, L., Ellis, J., Crisp, P., Cook, A., 1983. Comparative study of oil shales and shale oils from the mahogany zone, green river formation (usa) and kerosene creek seam, rundle formation (australia). Chemical Geology 38, 185–212.

Instruments, J., 2011. Qitm mode-quantitative imaging with the nanowizard 3 afm. Tech. Note (JPK Instruments), 1–7.

Jarvie, D., Pollastro, R., Hill, R., Bowker, K., Claxton, B., Burgess, J., 2004. Evaluation of hydrocarbon generation and storage in the barnett shale, ft. worth basin, texas, in: Ellison Miles Memorial Symposium, Farmers Branch, Texas, USA, pp. 22–23.

Khatibi, S., Ostadhassan, M., Tuschel, D., Gentzis, T., Bubach, B., Carvajal-Ortiz, H., 2018. Raman spectroscopy to study thermal maturity and elastic modulus of kerogen. International Journal of Coal Geology 185, 103–118.

Kossovich, E., Dobryakova, N., Epshtein, S., Belov, D., 2016. Mechanical properties of coal microcomponents under continuous indentation. Journal of Mining Science 52, 906–912.

Laxminarayana, C., Crosdale, P.J., 1999. Role of coal type and rank on methane sorption characteristics of bowen basin, australia coals. International Journal of Coal Geology 40, 309–325.

Leeder, M., 1988. Recent developments in carboniferous geology: a critical review with implications for the british isles and nw europe. Proceedings of the Geologists' Association 99, 73–100.

Levine, J.R., 1996. Model study of the influence of matrix shrinkage on absolute permeability of coal bed reservoirs. Geological Society, London, Special Publications 109, 197–212.

Li, C., Ostadhassan, M., Guo, S., Gentzis, T., Kong, L., 2018. Application of peakforce tapping mode of atomic force microscope to characterize nanomechanical properties of organic matter of the bakken shale. Fuel 233, 894–910.

Li, C., Ostadhassan, M., Kong, L., Bubach, B., 2019. Multi-scale assessment of mechanical properties of organic-rich shales: A coupled nanoindentation, deconvolution analysis, and homogenization method. Journal of Petroleum Science and Engineering 174, 80–91.

Li, W., Cheng, Y.p., Wang, L., Zhou, H.x., Wang, H.f., Wang, L.g., 2013. Evaluating the security of geological coalbed sequestration of supercritical co2 reservoirs: the haishiwan coalfield, china as a natural analogue. International Journal of Greenhouse Gas Control 13, 102–111.

Li, Y., Yang, J., Pan, Z., Tong, W., 2020. Nanoscale pore structure and mechanical property analysis of coal: An insight combining afm and sem images. Fuel 260, 116352.

Liu, H., Lin, B., Yang, W., 2019. Theoretical models for gas adsorption-induced coal deformation under coal seam field conditions. Energy Science & Engineering 7, 1504–1513.

Liu, J., Chen, Z., Elsworth, D., Miao, X., Mao, X., 2010. Linking gas-sorption induced changes in coal permeability to directional strains through a modulus reduction ratio. International Journal of Coal Geology 83, 21–30.

Liu, K., Ostadhassan, M., Bubach, B., Ling, K., Tokhmechi, B., Robert, D., 2018. Statistical grid nanoindentation analysis to estimate macro-mechanical properties of the bakken shale. Journal of Natural Gas Science and Engineering 53, 181–190.

Ma, Q., Harpalani, S., Liu, S., 2011. A simplified permeability model for coalbed methane reservoirs based on matchstick strain and constant volume theory. International Journal of Coal Geology 85, 43–48.

Masoudian, M.S., 2016. Multiphysics of carbon dioxide sequestration in coalbeds: A review with a focus on geomechanical characteristics of coal. Journal of Rock Mechanics and Geotechnical Engineering 8, 93–112.

Mastalerz, M., Karayigit, A., Hampton, L., Drobniak, A., 2016. Variations in gas content in organic matter-rich low maturity shale; example from the new albany shale in the illinois basin. Jacobs Journal of Petroleum and Natural Gas 1, 005.

Mastalerz, M., Rupp, J., Drobniak, A., Harpalani, S., Anderson, A., Korose, C., Frailey, S., Morse, D., 2009. Assessment of co2 sequestration and enhanced coalbed methane potential in unminable coal seams of the illinois basin .

Mathieson, A., Midgley, J., Dodds, K., Wright, I., Ringrose, P., Saoul, N., 2010. Co 2 sequestration monitoring and verification technologies applied at krechba, algeria. The Leading Edge 29, 216–222.

Morcote, A., Mavko, G., Prasad, M., 2010. Dynamic elastic properties of coal. Geophysics 75, E227 –E234.

More, J., 1977. The levenberg-marquardt algorithm: implementation and theory numerical analysis (lecture notes in mathematics vol 630) ed ga watson.

Murchison, D., 2004. Aberrations in the coalification patterns of the offshore coalfields of northumberland and durham, united kingdom. International journal of coal geology 58, 133 –146.

O'Keefe, J.M., Bechtel, A., Christanis, K., Dai, S., DiMichele, W.A., Eble, C.F., Esterle, J.S., Mastalerz, M., Raymond, A.L., Valentim, B.V., et al., 2013. On the fundamental difference between coal rank and coal type. International Journal of Coal Geology 118, 58–87.

Palmer, I., Mansoori, J., et al., 1996. How permeability depends on stress and pore pressure in coalbeds: a new model, in: SPE annual technical conference and exhibition, Society of Petroleum Engineers.

Pan, J., Meng, Z., Hou, Q., Ju, Y., Cao, Y., 2013. Coal strength and young's modulus related to coal rank, compressional velocity and maceral composition. Journal of Structural Geology 54, 129–135.

Pan, Z., Connell, L.D., 2007. A theoretical model for gas adsorption-induced coal swelling. International Journal of Coal Geology 69, 243–252.

Pan, Z., Connell, L.D., Camilleri, M., 2010. Laboratory characterisation of coal reservoir permeability for primary and enhanced coalbed methane recovery. International Journal of Coal Geology 82, 252 –261.

Pittenger, B., Erina, N., Su, C., 2014. Mechanical property mapping at the nanoscale using peakforce qnm scanning probe technique, in: Nanomechanical analysis of high performance materials. Springer, pp. 31–51.

Ranathunga, A.S., Perera, M.S.A., Ranjith, P., Bui, H., 2016. Super-critical co2 saturation-induced mechanical property alterations in low rank coal: An experimental study. The Journal of Supercritical Fluids 109, 134–140.

Ranjith, P., Perera, M.S.A., 2012. Effects of cleat performance on strength reduction of coal in co2 sequestration. Energy 45, 1069–1075.

Rexer, T.F., Mathia, E.J., Aplin, A.C., Thomas, K.M., 2014. High-pressure methane adsorption and characterization of pores in posidonia shales and isolated kerogens. Energy & Fuels 28, 2886 –2901.

Ringrose, P., Atbi, M., Mason, D., Espinassous, M., Myhrer, Ø., Iding, M., Mathieson, A., Wright, I., 2009. Plume development around well kb-502 at the in salah co2 storage site. First break 27.

Robertson, E.P., 2005. Measurement and modeling of sorption-induced strain and permeability changes in coal. Technical Report. Idaho National Laboratory (INL).

Shi, J., Durucan, S., 2004. Drawdown induced changes in permeability of coalbeds: a new interpretation of the reservoir response to primary recovery. Transport in porous media 56, 1–16.

Sneddon, I.N., 1965. The relation between load and penetration in the axisymmetric boussinesq problem for a punch of arbitrary profile. International journal of engineering science 3, 47–57.

Stach, E., Murchison, D., Taylor, G.H., Zierke, F., 1982. Stach's textbook of coal petrology. volume 535. Borntraeger Berlin.

Standard, A., et al., 2014. Standard test method for microscopical determination of the reflectance of vitrinite dispersed in sedimentary rocks .

Stephen, C., Passey, Q.R., 1993. Recurring patterns of total organic carbon and source rock quality within a sequence stratigraphic framework. AAPG bulletin 77, 386–401.

Strapoc, D., Mastalerz, M., Schimmelmann, A., Drobniak, A., Hasenmueller, N.R., 2010. Geochemical constraints on the origin and volume of gas in the new albany shale (devonian–mississippian), eastern illinois basin. AAPG bulletin 94, 1713–1740.

Taylor, G.H., Teichmüller, M., Davis, A., Diessel, C., Littke, R., Robert, P., 1998. Organic petrology .

Teichmüller, M., 1989. The genesis of coal from the viewpoint of coal petrology. International Journal of Coal Geology 12, 1 – 87. http://www.sciencedirect.com/science/article/pii/0166516289900475, https://doi.org/10.1016/0166-5162(89)90047-5.

Turner, B.R., Richardson, D., 2004. Geological controls on the sulphur content of coal seams in the northumberland coalfield, northeast england. International Journal of Coal Geology 60, 169–196.

Ulm, F.J., Abousleiman, Y., 2006. The nanogranular nature of shale. Acta Geotechnica 1, 77–88.

Ulm, F.J., Vandamme, M., Bobko, C., Alberto Ortega, J., Tai, K., Ortiz, C., 2007. Statistical indentation techniques for hydrated nanocomposites: concrete, bone, and shale. Journal of the American Ceramic Society 90, 2677–2692.

Viete, D.R., Ranjith, P.G., 2006. The effect of co2 on the geomechanical and permeability behaviour of brown coal: implications for coal seam co2 sequestration. International journal of coal geology 66, 204–216.

Wang, K., Xu, T., Wang, F., Tian, H., 2016. Experimental study of co2–brine–rock interaction during co2 sequestration in deep coal seams. International Journal of Coal Geology 154, 265–274.

Weber, M., Wilson, T.H., Akwari, B., Wells, A.W., Koperna, G., 2012. Impact of geological complexity of the fruitland formation on combined co2 enhanced recovery/sequestration at san juan basin pilot site. International journal of coal geology 104, 46–58.

West, L.M., 2014. A regional assessment of residual oil zones in the permian basin and their potential for carbon dioxide capture usage and storage. Energy Procedia 63, 7884–7890.

Yu, H., Zhang, Y., Lebedev, M., Han, T., Verrall, M., Wang, Z., Al-Khdheeawi, E., Al-Yaseri, A., Iglauer, S., 2018. Nanoscale geomechanical properties of western australian coal. Journal of Petroleum Science and Engineering 162, 736–746.

Zaluski, W., El-Kaseeh, G., Lee, S.Y., Piercey, M., Duguid, A., 2016. Monitoring technology ranking methodology for co2-eor sites using the weyburn-midale field as a case study. International Journal of Greenhouse Gas Control 54, 466–478.

Zhang, H., Liu, J., Elsworth, D., 2008. How sorption-induced matrix deformation affects gas flow in coal seams: a new fe model. International Journal of Rock Mechanics and Mining Sciences 45, 1226–1236.

Zhang, Y., Lebedev, M., Al-Yaseri, A., Yu, H., Xu, X., Iglauer, S., 2018a. Characterization of nanoscale rockmechanical properties and microstructures of a chinese sub-bituminous coal. Journal of Natural Gas Science and Engineering 52, 106–116.

Zhang, Y., Lebedev, M., Al-Yaseri, A., Yu, H., Xu, X., Sarmadivaleh, M., Barifcani, A., Iglauer, S., 2018b. Nanoscale rock mechanical property changes in heterogeneous coal after water adsorption. Fuel 218, 23–32.

Zhang, Y., Zhang, Z., Sarmadivaleh, M., Lebedev, M., Barifcani, A., Yu, H., Iglauer, S., 2017. Micro-scale fracturing mechanisms in coal induced by adsorption of supercritical co2. International Journal of Coal Geology 175, 40–50.

Zheng, Z., Khodaverdian, M., McLennan, J., 1991. Static and dynamic testing of coal specimens, in: 1991 SCA Conference.